iScience

CellPress
OPEN ACCESS

Article

Dendritic Kv4.2 potassium channels selectively mediate spatial pattern separation in the dentate gyrus

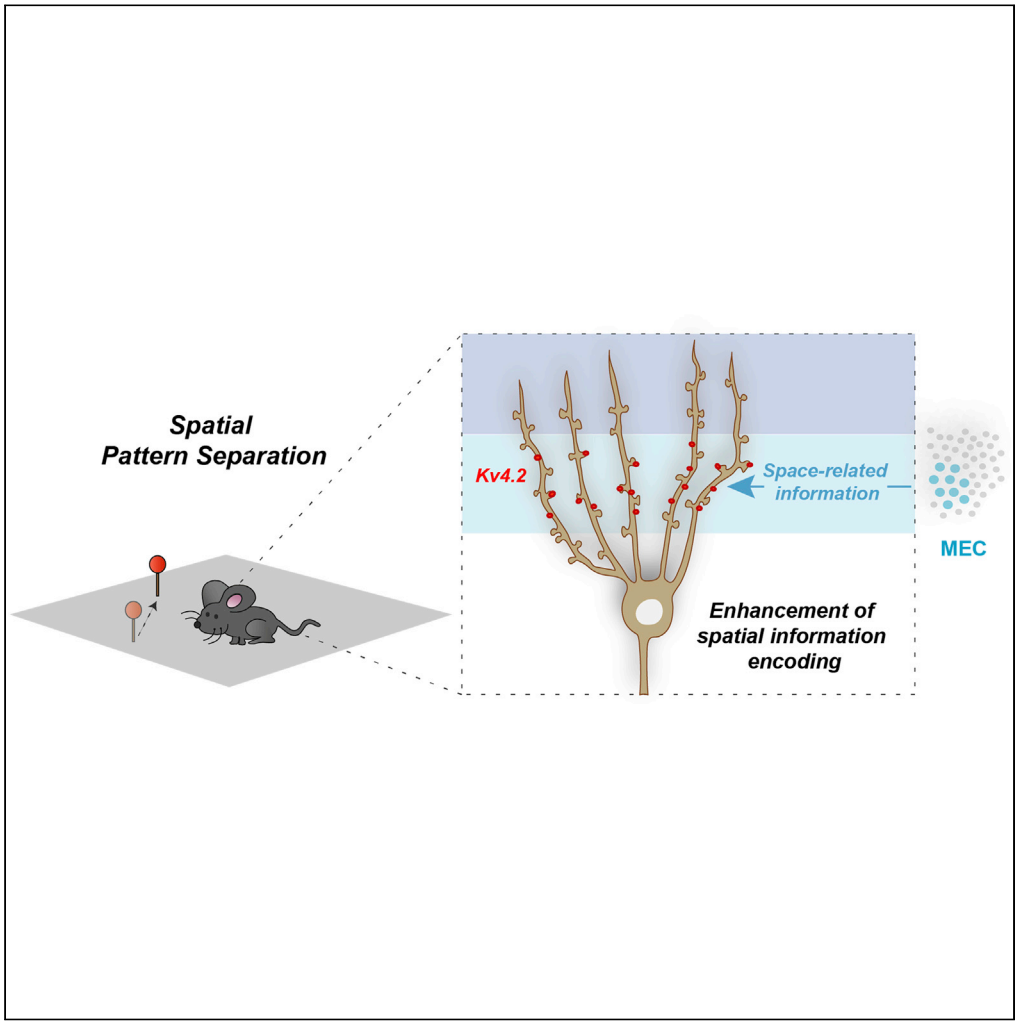

Marie Oulé, Erika Atucha, Tenyse M. Wells, Tamar Macharadze, Magdalena M. Sauvage, Michael R. Kreutz, Jeffrey Lopez-Rojas

jl5545@columbia.edu

Highlights

The Kv4.2 channel decreases the excitability of medial dendrite synapses in GCs

The Kv4.2 channel dampens the amplitude of bAPs in medial dendrites of GCs

Intrinsic plasticity of medial perforant path DG is occluded in the absence of Kv4.2

The Kv4.2 knockout results in a specific impairment of spatial pattern separation

Oulé et al., iScience 24, 102876
August 20, 2021
https://doi.org/10.1016/j.isci.2021.102876

iScience

CellPress
OPEN ACCESS

Article

Dendritic Kv4.2 potassium channels selectively mediate spatial pattern separation in the dentate gyrus

Marie Oulé,[1] Erika Atucha,[2] Tenyse M. Wells,[2] Tamar Macharadze,[1,3] Magdalena M. Sauvage,[2,4,5] Michael R. Kreutz,[1,5,6,7] and Jeffrey Lopez-Rojas[1,5,8,9,*]

SUMMARY

The capacity to distinguish comparable experiences is fundamental for the recall of similar memories and has been proposed to require pattern separation in the dentate gyrus (DG). However, the cellular mechanisms by which mature granule cells (GCs) of the DG accomplish this function are poorly characterized. Here, we show that Kv4.2 channels selectively modulate the excitability of medial dendrites of dentate GCs. These dendrites are targeted by the medial entorhinal cortex, the main source of spatial inputs to the DG. Accordingly, we found that the spatial pattern separation capability of animals lacking the Kv4.2 channel is significantly impaired. This points to the role of intrinsic excitability in supporting the mnemonic function of the dentate and to the Kv4.2 channel as a candidate substrate promoting spatial pattern separation.

INTRODUCTION

Memory of daily events is stored in the hippocampus. As these events might share important features, hippocampal processes lowering the interferences are essential for accurate recall of the associated memories. Pattern separation refers to the ability to reduce the overlap between similar inputs in order to increase the probability of storing them as distinct memories. Compelling evidence proposes pattern separation as a hallmark of the dentate gyrus (DG). This assumption is mainly based on computational theory and behavioral observations, but direct cellular empirical facts demonstrating pattern separation in the DG are scarce (Aimone et al., 2011; Amaral et al., 2007; Chavlis et al., 2017; GoodSmith et al., 2017; Jung and McNaughton, 1993; Kesner and Rolls, 2015; Knierim and Neunuebel, 2016; Leutgeb et al., 2007; Marr, 1971; McHugh et al., 2007; Schmidt et al., 2012). While to date most of the studies have focused on understanding the neuronal circuitry supporting pattern separation, its cellular and molecular mechanisms remain largely unknown (Bekinschtein et al., 2013; Danielson et al., 2016; Espinoza et al., 2018; Kannangara et al., 2015; Knierim and Neunuebel, 2016; Madar et al., 2019; Schmidt et al., 2012). The medial and lateral entorhinal cortices are the major source of cortical efferents to the hippocampus, targeting the medial or distal dendrites of the DG granule cells (GCs), respectively (Amaral et al., 2007; Witter, 2007). While the medial entorhinal cortex (MEC) preferentially processes spatial information (Tennant et al., 2018), the lateral entorhinal cortex (LEC) is rather associated with the processing of non-spatial, object-related information (Beer et al., 2013; Eichenbaum et al., 2007; Knierim James et al., 2014; Sauvage et al., 2013; Wang et al., 2018). However, it is at present unclear whether distinct postsynaptic players are underlying the processing of LEC or MEC inputs in the DG.

Mature GCs are weakly excitable neurons that rarely fire action potentials (Alme et al., 2010; Jung and McNaughton, 1993; Pernia-Andrade and Jonas, 2014; Staley et al., 1992), a feature associated to their sparse coding (Knierim and Neunuebel, 2016; Yassa and Stark, 2011). The ability of a neuron to integrate synaptic inputs and to fire action potentials is tightly regulated by its intrinsic excitability (Debanne et al., 2019), which is shaped by the subcellular expression and activity of ion channels that can have a non-homogenous distribution across dendritic domains (Duménieu et al., 2017; Frick and Johnston, 2005; Lai and Jan, 2006; Remy et al., 2010; Titley et al., 2017; Trimmer, 2015). Although poorly studied, mature GC dendrites have been described as strong passive attenuators of synaptic inputs (Krueppel et al., 2011). However, electrical stimulation that fails to induce synaptic plasticity in mature GCs can positively affect their dendritic excitability putatively through modulation of dendritic A-type channels

[1]Research Group Neuroplasticity, Leibniz Institute for Neurobiology, 39118 Magdeburg, Germany

[2]Functional Architecture of Memory Department, Leibniz Institute for Neurobiology, 39118 Magdeburg, Germany

[3]Department of Anesthesiology and Intensive Care Medicine, Otto-von-Guericke-University, 39120 Magdeburg, Germany

[4]Otto von Guericke University, Medical Faculty, Functional Neuroplasticity Department, 39120, Magdeburg, Germany

[5]Center for Behavioral Brain Sciences (CBBS), 39106 Magdeburg, Germany

[6]Leibniz Group 'Dendritic Organelles and Synaptic Function', University Medical Center Hamburg-Eppendorf, Center for Molecular Neurobiology (ZMNH), 20251 Hamburg, Germany

[7]German Center for Neurodegenerative Diseases (DZNE), 39120 Magdeburg, Germany

[8]Department of Neuroscience, The Kavli Institute for Brain Science, Mortimer B. Zuckerman Mind Brain Behavior Institute, Vagelos College of Physicians and Surgeons, Columbia University, New York, NY 10027, USA

[9]Lead contact

*Correspondence: jl5545@columbia.edu

https://doi.org/10.1016/j.isci.2021.102876

(Lopez-Rojas et al., 2016). This puts forward intrinsic excitability regulation as a key phenomenon allowing mature GCs to overcome their poor synaptic plasticity properties (Schmidt-Hieber et al., 2004) and to promote synaptic signal integration necessary for memory formation. Hence, the local regulation of voltage-gated ion channels is an appealing mechanism to differentially process synaptic signals in an input-specific manner.

The A-type potassium channel is a well-known regulator of dendritic excitability (Hoffman et al., 1997; Kim et al., 2005; Watanabe et al., 2002; Yang et al., 2015), whose activity is tightly regulated by synaptic activity (Frick et al., 2004; Kim et al., 2007). In GCs, the A-current is mediated by both Kv4.2 and Kv4.3 channels (Monaghan et al., 2008). However, their role in the dendritic integration of GCs is controversial (Kim et al., 2018; Krueppel et al., 2011; Lopez-Rojas et al., 2016; Truchet et al., 2012). Therefore, we first aimed at determining the influence of the Kv4.2 and Kv4.3 channels in the intrinsic properties of the mature GCs and their relative contribution to the integration of MEC and LEC inputs. Furthermore, we sought to understand how the lack of these channels affected the spatial and non-spatial pattern separation capability of the animals.

RESULTS

The absence of Kv4.2 channels is associated with enhanced dendritic excitability in response to medial, but not lateral, perforant path stimulation

As entorhinal inputs are anatomically segregated, it is possible to study their integration independently by placing a stimulation electrode in the vicinity of medial (MEC inputs) or distal (LEC inputs) GC dendrites (Figure S1). The impact of A-type potassium channels on the ability of dendrites to convey excitatory post-synaptic potentials (EPSPs) to the soma was studied in basal condition in the presence of bicuculline in order to isolate the A-type channel contribution to the intrinsic excitability of the GCs. To this end, we patched mature GCs and measured the amplitude/slope relation of the evoked subthreshold EPSPs, i.e. EPSPs that do not trigger somatic action potentials , as well as the EPSP slope needed to make a cell fire an action potential with 50% probability, that is, the threshold EPSP (E50). Whereas the slope of the EPSP during the first couple of milliseconds is controlled by the synaptic drive, i.e., the number and properties of α-amino-3-hydroxy-5-methyl-4-isoxazolepropionic acid (AMPA) receptors opening at the synapse, the amplitude of the EPSP is also modulated by slower dendritic voltage-gated ion channels. Therefore, EPSPs with comparable slopes (equal synaptic drive) in different experimental conditions might have different amplitudes based on the ion channels opening upon membrane depolarization, thus reflecting differences in the intrinsic excitability of dendrites. Changes in EPSP amplitude would consequently impact on the ability of the cells to fire action potentials in response to a given synaptic input: whereas the action potential threshold would be reached with high probability in the case of a large EPSP amplitude, an EPSP with a small amplitude would hardly reach the threshold for action potential generation. A-type potassium channels need the depolarization provided by the opening of the AMPA receptors to open during a synaptic event. A-type channels then produce a hyperpolarizing transient current that dampens the EPSP amplitude without affecting much the initial rising phase/slope of the EPSP.

After medial perforant path stimulation, mature GCs from both Kv4.2 and Kv4.3 knockout mice showed significantly larger EPSP-amplitude/slope ratios—here reported as the slope of the linear fit of the EPSP-amplitude vs. EPSP-slope relation—than controls (Figures 1 and S2). On average, EPSPs from Kv4.2 knockout mice were roughly 14% larger than control values (Figures 1B and 1D, $t(93) = 3.703$ $p = 0.0004$, t test), whereas Kv4.3 knockout mice EPSPs were larger by 9% (Figure S2B, $t(94) = 2.020$ $p = 0.0462$, t test). EPSPs from Kv4.2 knockout mice exceeded control values by approximately 2 mV around the range of EPSP slopes needed to fire action potentials (Figure 1C $F(1, 84) = 12.01$ $p = 0.0008$ for the factor genotype, $F(1, 84) = 69.92$ $p < 0.0001$ for the factor "EPSP-amplitude", and $F(1, 84) = 0.1841$ $p = 0.6690$ for the Interaction genotype x "EPSP-amplitude", repeated measures two-way analysis of variance [ANOVA]). The increased EPSP amplitude in Kv4.2 knockout mice translated into a significant reduction of the EPSP threshold (Figures 1B and 1E, $t(90) = 2.309$ $p = 0.0232$, t test) suggesting a better synapse-to-soma electrical communication, while Kv4.3 knockout cells showed only a trend to lower EPSP threshold values (Figure S2B, $t(90) = 1.482$ $p = 0.1418$, t test). Similar changes were observed after pharmacological blockade of A-type channels with 4-aminopyridine (4-AP, EPSP-amplitude/slope ratios in 4-AP and control groups: 5.026 ± 0.3192 ms and 3.208 ± 0.1741 ms, respectively; $t(34) = 5.000$ $p < 0.0001$, t test. EPSP threshold in 4-AP and control groups: 3.888 ± 0.2769 Vs^{-1} and 6.937 ± 0.4163 Vs^{-1}, respectively; $t(33) = 6.165$ $p < 0.0001$, t test).

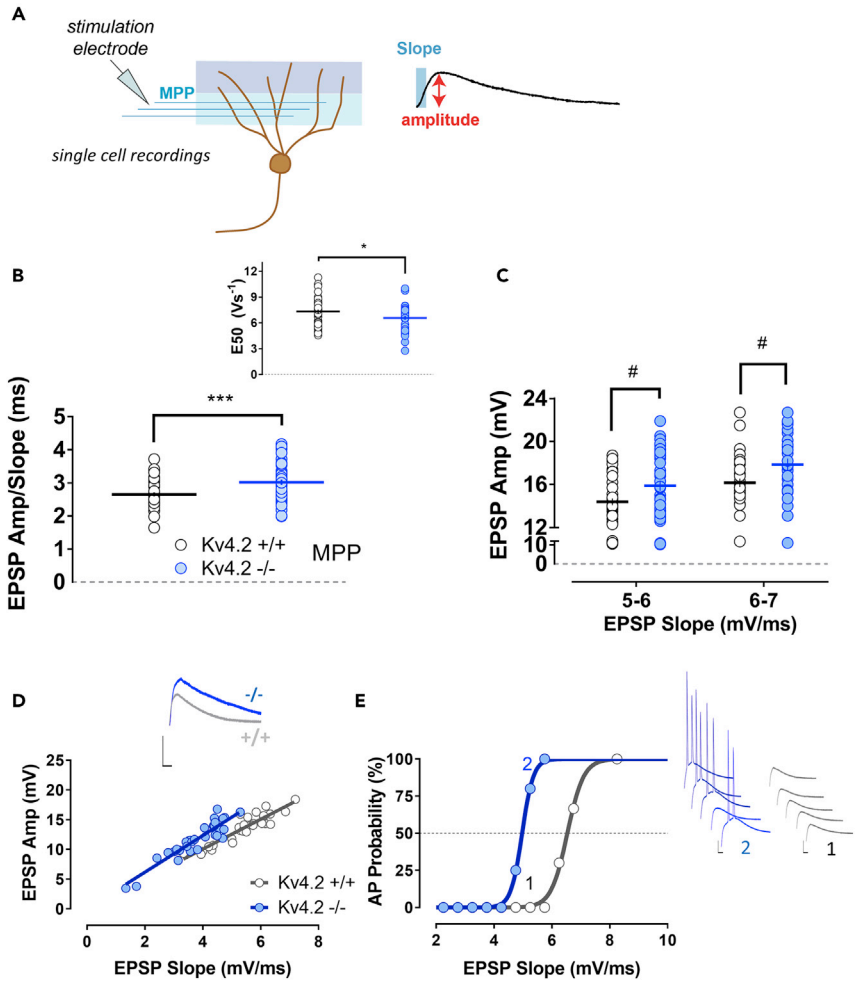

Figure 1. Enhanced excitability of mature GCs of Kv4.2 knockout mice in response to medial perforant path synaptic stimulation

(A) Scheme showing the positioning of the extracellular stimulation electrode at the middle of the molecular layer in order to stimulate the medial perforant path while recording electrical activity from single mature GCs through the patch-clamp technique.

(B) GCs from Kv4.2 knockouts (n = 48) show, for a given EPSP slope, EPSPs of significantly larger amplitude than controls (n = 47). Insets show illustrative EPSP traces, as well as a statistically significant reduction in the EPSP threshold (EPSP slope needed to fire an action potential with 50% probability) in Kv4.2 knockouts.

(C) The EPSP amplitudes were significantly larger for Kv4.2 knockouts around the critical range of EPSP slopes needed to fire an action potential with 50% probability.

(D) An illustrative example of the amplitude/slope relation of subthreshold EPSPs for a Kv4.2 knockout and a wild-type cell. For a given EPSP slope, the amplitude of the EPSP is increased in the knockout cell. Solid lines show linear fits for each group (slopes of the fitted lines: wild type 2.511 $\pm$ 0.03262 ms and knockout 3.083 $\pm$ 0.05248 ms).

(E) Example of a plotting of the firing probability versus EPSP slope for a wild-type and a Kv4.2 knockout cell. There is an increased firing probability for a given EPSP slope in the knockout cell. All recordings were made in the presence of bicuculline. Data are represented as mean $\pm$ SEM. Scale bars represent 10 mV/10 ms. *: $p < 0.05$, ***: $p < 0.001$, t test. #: $p < 0.05$, ANOVA.

Next, for testing the possibility that the enhanced ability of EPSPs to elicit action potentials in the knockout animals was due to a modification of the dendritic excitability—rather than due to some general somatic excitability changes—the firing properties of mature GCs in response to somatic depolarization were also investigated. Neurons from Kv4.2 knockout mice were undistinguishable from controls regarding the number of action potentials (Figures 2A and 2B), the minimum current needed to elicit action potentials (rheobase, Figure 2C), their input resistance (Figure 2D), action potential amplitude (Figures 2E and 2F), threshold (Figure 2G), or width (Figure 2H). Similarly, mature GCs from Kv4.3 knockout mice displayed a

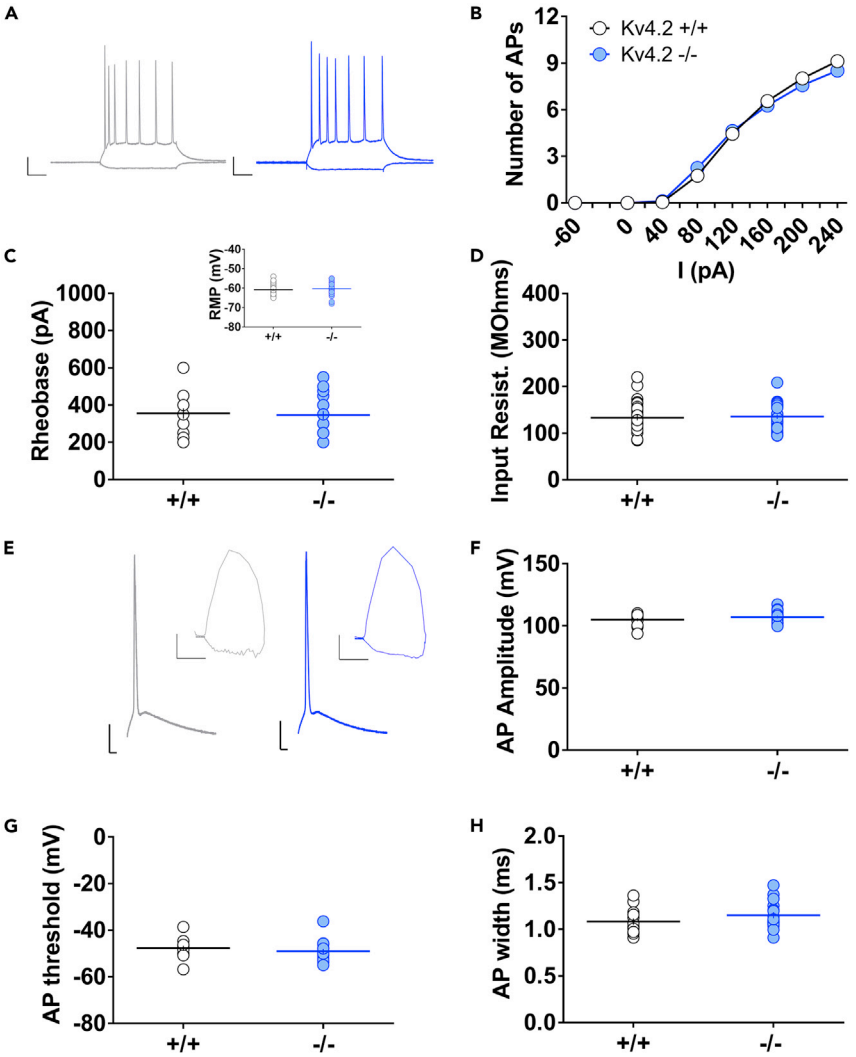

Figure 2. Kv4.2 knockout does not alter the general somatic excitability of mature dentate GCs

(A–D) (A) Representative traces showing the firing of mature GCs in response to a 250-ms-long square pulse current injection to the soma. Scale bars, 20 mV/50 ms. Neither the number of action potentials (B) nor the minimum current needed to elicit an action potential (i.e. rheobase), (C) nor the input resistance or resting membrane potential of the cell, (D) were modified in Kv4.2 knockout mice.

(E–H) (E) Representative traces showing the firing of mature GCs in response to a 5-ms-long square pulse current injection to the soma. Scale bars, 20 mV/4 ms. Also shown are the phase plots of the action potentials. Scale bars, 100 $mV*ms^{-1}$/50 mV. Neither the action potential amplitude (F) nor the action potential threshold, (G) nor the action potential width, (H) were modified. (Kv4.2 −/− n = 19, Kv4.2 +/+ n = 15). Data are represented as mean ± SEM

comparable somatic excitability to those of control cells (Figure S3), except for the slightly wider action potential (Figure S3H, t(50) = 2.162 p = 0.0355, t test). Moreover, no major changes in the neuronal morphology or spine density were observed in mature GCs of Kv4.2 (Figure 3) or Kv4.3 knockouts (Figure S4). These results suggest that the alterations of intrinsic excitability observed after medial perforant path synaptic stimulation were not due to global somatic excitability changes or gross morphological alterations but rather to local modifications of dendritic intrinsic excitability mediated by the Kv4.2 channel.

After lateral perforant path stimulation, Kv4.2 knockout cells showed a surprisingly reduced dendritic excitability with smaller EPSP-amplitude/slope ratios and an increased EPSP threshold compared to controls (Figure S5B, EPSP-amplitude/slope: t(64) = 2.284 p = 0.0257, t test, EPSP threshold: t(55) = 3.047 p = 0.0036, t test). The Kv4.3 knockouts on the other hand did not differ from control cells (Figure S5C,

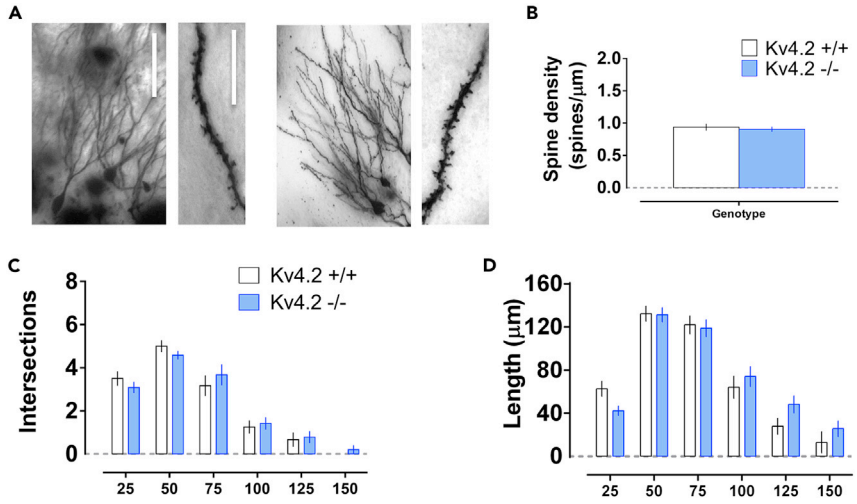

Figure 3. Loss of Kv4.2 channels does not affect the general morphology of mature dentate GCs

(A) Golgi-stained dentate GCs of wild-type (left) and Kv4.2 knockout mice (right). The spine density in medial dendrites was similar in both genotypes.

(B–D) (B).Dendritic branching was examined using Sholl analysis. Neither the number of crossings (C) nor the dendritic length (D) differed between genotypes. Data are represented as mean ± SEM. Scale bars, 50 µm or 20 µm for wide field view of cells or enlarged image of spines, respectively. n = 12 for every genotype.

EPSP-amplitude/slope: t(89) = 0.7264 p = 0.4695, t test; EPSP threshold: t(86) = 1.650 p = 0.1026, t test). Moreover, bath application of the potassium channel blocker 4-AP resulted in an overall enhanced intrinsic excitability of mature cells (EPSP-amplitude/slope ratios in 4-AP and control groups: 7.046 ± 0.3465 ms and 5.229 ± 0.2126 ms, respectively; t(33) = 4.409 p = 0.001, t test. EPSP threshold in 4-AP and control groups: 2.513 ± 0.1392 Vs^{-1} and 3.858 ± 0.1713 Vs^{-1}, respectively; t(33) = 6.127 p < 0.0001, t test). The reduced excitability of Kv4.2 knockout cells in response to lateral perforant path stimulation contradicts expected results following gene knockout of a dendritic hyperpolarizing channel and contrasts with what was observed after 4-AP application. Potentially, because the DG is a well-known niche of epileptic seizure (Koyama, 2016), the negative regulation of the distal dendrite's excitability might reflect a homeostatic response counterbalancing the hyperexcitability measured in the medial dendrites.

We next used cFos-green fluorescent protein (GFP) reporter mice (Barth et al., 2004) to investigate potential modifications of mature GCs excitability induced by physiological stimuli. To this end, cFos-GFP animals were exposed to 30 min of enriched environment (EE). Patch-clamp recordings of experience-activated (GFP positive) and non-activated (GFP negative) neighbor cells were realized after EE (Figure 4). Interestingly, in activated mature GCs, the brief exposure to EE elicited similar excitability changes as those observed in medial dendrites of the Kv4.2 knockout animals. We found that the experience-activated cells have significantly larger EPSPs in response to medial perforant path stimulation than non-activated neighbor cells (Figures 4B and 4C, t(23) = 2.650 p = 0.0143, paired t test "activated GC" vs. "non-activated neighbor GC"). The enhancement of the EPSP propagation translated into an increased ability of medial perforant path-evoked EPSPs to elicit action potentials in activated mature GCs (Figures 4B and 4D, t(23) = 2.513 p = 0.0194, paired t test). On the contrary, no changes in the EPSP propagation or integration were observed after stimulation of the lateral perforant path inputs (Figure S6, EPSP-amplitude/slope: t(16) = 0.8617 p = 0.4016 and EPSP threshold: t(14) = 1.597 p = 0.1325, paired t test). Therefore, physiological stimuli mimic the alterations in intrinsic excitability observed in the Kv4.2 knockout animals and thus primarily impact the processing of medial, rather than lateral, perforant path inputs.

Collectively, these results point to A-type potassium channels and here mainly Kv4.2 channels, as important input-specific regulators of the excitability of mature GCs particularly at dendritic segments receiving input from the medial perforant path. Interestingly, experience also affects the intrinsic properties of medial dendrites, suggesting that medial perforant path inputs might be the first whose integration is modulated potentially through regulation of the activity of the Kv4.2 channel.

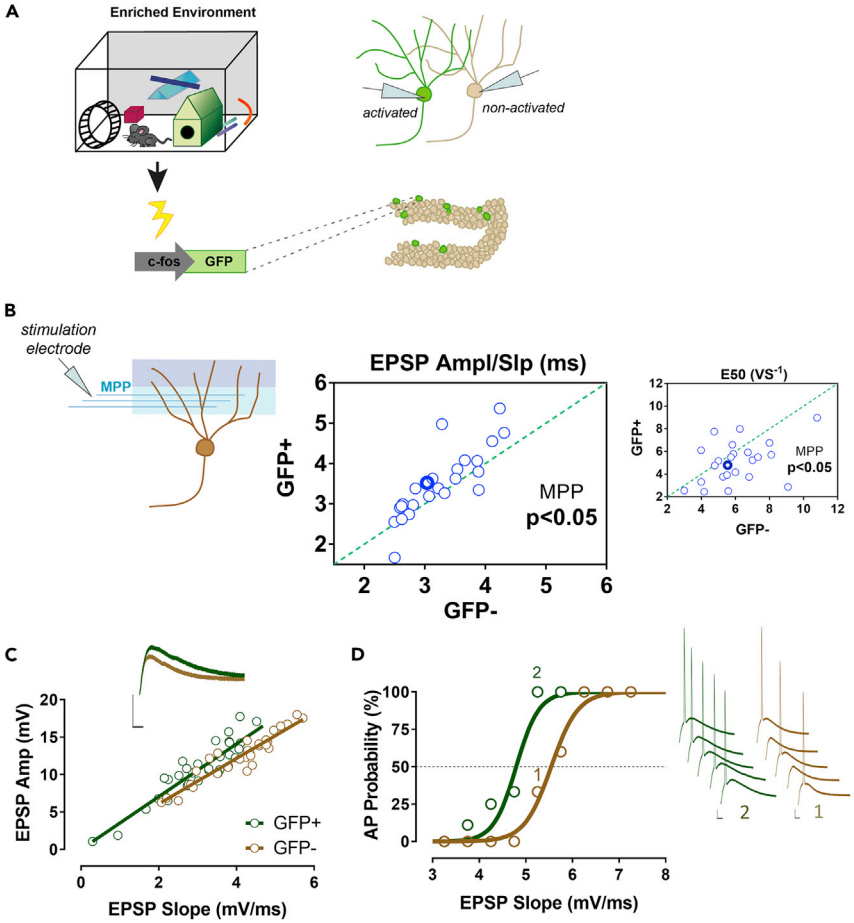

Figure 4. Mature GCs activated during a short exposure to an enriched environment show an enhanced intrinsic excitability, mimicking the phenotype of the Kv4.2 knockout neurons

(A) cFos-GFP reporter mice were used to target mature GCs activated by the enriched environment experience. Electrophysiological recordings were obtained from GFP-positive cells (activated) and GFP-negative (non-activated) neighbor cells.

(B) Activated mature GCs show, for a given EPSP slope, EPSPs of significantly larger amplitude than non-activated neighbor cells after medial perforant path stimulation as well as a smaller EPSP threshold compared to controls (n = 24).

(C) An illustrative example of the amplitude/slope relation of subthreshold EPSPs for a GFP-positive and a neighbor GFP-negative cell. For a given EPSP slope, the amplitude of the EPSP is increased in the GFP-positive cell.

(D) Example of a plotting of the firing probability versus EPSP-slope for a GFP-positive and a neighbor GFP-negative cell. There is an increased firing probability for a given EPSP slope in the GFP-positive cell. All recordings were made in the presence of bicuculline. Scale bars, 10 mV/10 ms.

Enhanced backpropagation of action potentials into medial dendrites of Kv4.2 knockouts

A-type potassium channels can also open after the depolarization induced by the backpropagating action potential (bAP) significantly reducing its amplitude (Hoffman et al., 1997). The influence of the Kv4.2 and Kv4.3 channels in modulating the bAP was assessed by filling mature GCs with the calcium indicator Fluo-5F. With help of two-photon microscopy, the calcium influx elicited by the bAP-mediated membrane depolarization along the dendritic tree of mature GCs was measured (Figure 5A). Interestingly, the calcium influx in the medial dendritic segment of mature cells was larger in Kv4.2 knockout cells than in controls. The difference reached statistical significance for dendritic stretches that were around 75–100 μm farther from the soma, where the calcium transients were roughly 2.5 times the control values (Figures 5B and 5F($9, 297) = 2.395 p = 0.0124 for the interaction genotype x "distance from soma" repeated measures two-way ANOVA, p = 0.0045, Sidak's multiple comparisons test). This enhancement of the calcium influx reflects a larger amplitude of the bAP in Kv4.2 knockout mature cells in a dendritic region where mainly medial

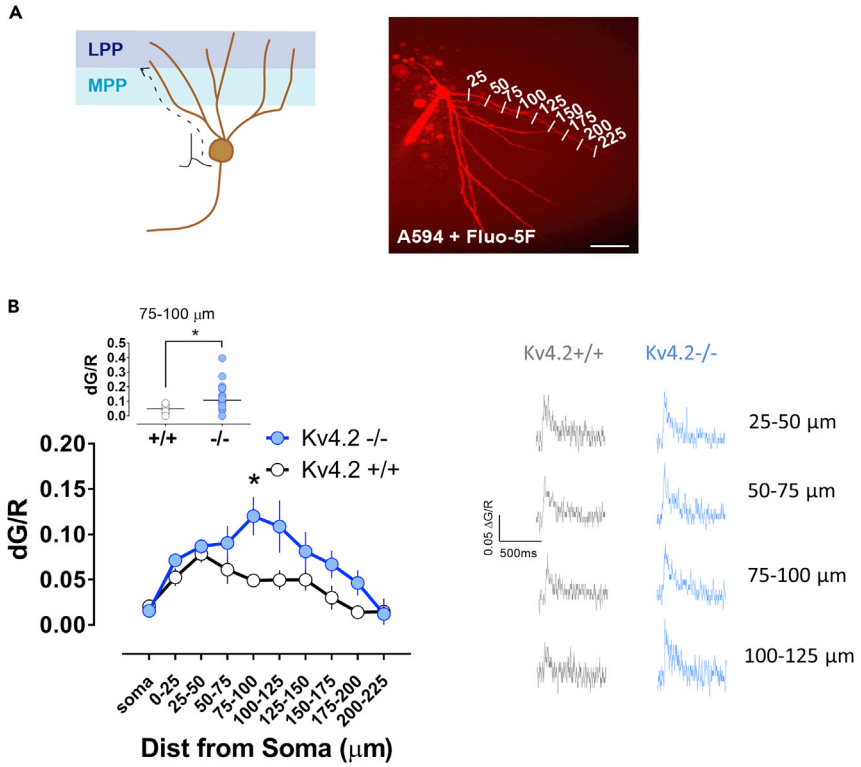

Figure 5. Kv4.2 knockout results in larger bAPs into medial dendrites of mature GCs

(A and B) (A) Scheme showing the backpropagation of the action potential from the soma to dendrites. Neurons were filled with Fluo-5F, and calcium transients were measured at different distances from the soma. Mature GCs of Kv4.2 knockouts (Kv4.2 −/− n = 20, Kv4.2 +/+ n = 14) showed an enhanced action potential backpropagation into medial dendrites (B). The insets in (B) show individual values for Kv4.2 wild-type and knockout cells at 75–100 µm from the soma, as well as representative calcium transients. All recordings were made in the presence of bicuculline. Scale bar in (A) 50 µm. Data are represented as mean ± SEM. *: $p < 0.05$, ANOVA.

perforant path synapses localize. Importantly, as the bAP amplitude was not affected in the proximal dendrites of Kv4.2 knockout cells, the boost observed in the medial dendrites cannot be explained by facilitation of the backpropagation in proximal dendrites. As the lack of Kv4.2 channels did not affect action potential properties in mature GCs (Figure 2), these data strengthen the hypothesis that the lack of Kv4.2 channels locally affects the excitability of the medial dendrites of mature GCs while the somatic properties remain preserved. Pharmacological blockade of A-type channels with 4-AP also resulted in an overall enhanced backpropagation of the action potential in mature GCs ($p = 0.014$, $p = 0.004$ and $p = 0.020$ for 75–100, 100–125, and 125–150 µm from soma, respectively, Sidak's multiple comparisons test after two-way ANOVA). However, mature cells of Kv4.3 knockout mice were in general similar to control cells (Figure S7), again pointing at a predominant modulatory effect of Kv4.2 but not Kv4.3 on dendritic excitability of mature GCs where the Kv4.2 channels limit the backpropagation of the action potential into their medial dendrites.

Occlusion of intrinsic plasticity after medial perforant path theta burst stimulation in mature GCs of Kv4.2 knockout mice

We have previously reported that the induction of synaptic plasticity after theta burst stimulation of the medial perforant path in mature GCs is accompanied by a surprisingly large increase in excitability that is occluded by the pharmacological blockade of A-type channels with 4-AP (Lopez-Rojas et al., 2016). These findings suggest that the downregulation of the A-type current is a regulatory mechanism for intrinsic plasticity. To test this hypothesis, we looked at the potential blockade of the theta burst stimulation-mediated intrinsic plasticity in mice lacking either the Kv4.2 or the Kv4.3 channels by stimulating the medial or lateral perforant path.

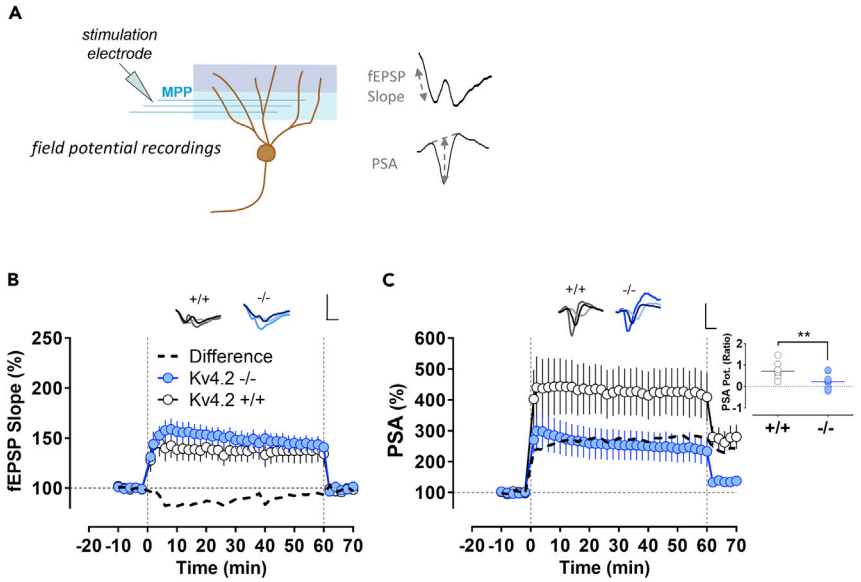

Figure 6. Occlusion of plasticity-induced excitability changes in Kv4.2 knockout mice after theta burst stimulation to the medial perforant path

(A–C) (A) Scheme showing the positioning of the extracellular stimulation electrode at the middle of the molecular layer in order to stimulate the medial perforant path while recording electrical activity from mature GCs. Time course of field EPSP slope (B) and population spike amplitude (PSA) (C). PSA and fEPSP values were normalized for every slice to the pre-conditioning baseline. The theta burst stimulation protocol was applied at time "0". One hour after the theta burst stimulation protocol, the test stimulation intensity was reduced to match the baseline fEPSP slope values. The remaining PSA potentiation is due to excitability changes independent of synaptic potentiation. GCs from Kv4.2 knockouts (Kv4.2 −/− n = 12, Kv4.2 +/+ n = 9) had impaired PSA potentiation, despite a normal fEPSP potentiation. Data are represented as mean ± SEM. Scale bars, 10 mV/10 ms. **: $p < 0.01$, t test.

For these experiments, a first electrode was placed at the medial or distal dendrites of the GCs (Figure 6A) to record the synaptic responses, i.e., the field-excitatory postsynaptic potential (fEPSP), and a second electrode was positioned close to the GC layer to record the population spike generated by the integration of fEPSPs. A stimulation electrode was accordingly placed to stimulate the medial or lateral perforant path (Figures 6A and S8–S10). As previously shown, upon activation of the medial perforant path, the theta burst protocol elicited a modest fEPSP (synaptic) potentiation of around 140% lasting for one hour, and this potentiation was accompanied by a large population spike amplitude (PSA) potentiation of roughly 400% (Figure 6). To dissect the relative contribution of the potentiation of excitatory synapses from excitability changes to the alterations in the PSA, we decreased the test stimulation intensity one hour after the theta burst stimulation in order to obtain fEPSP slope values similar in magnitude to those recorded at baseline. This allowed us to compare the response of neurons in the DG to the same excitatory drive before and after the theta burst. Most importantly, this adjustment of the stimulation intensity to match the fEPSP slope values recorded at baseline failed to bring the PSA back to baseline level (Figures 6B and 6C, $t(8) = 4.370$ $p = 0.0004$, paired t test). More than half of the PSA potentiation could not be explained by the synaptic potentiation but only by intrinsic plasticity reflecting a better electrical coupling between the synapse and the soma. Thus, in response to the same synaptic drive, wild-type GCs were able to fire much more efficiently after the theta burst stimulation protocol than observed in baseline, indicating a strengthening of the EPSP spike coupling. This profile of excitability was in stark contrast to what was found in Kv4.2 knockout animals. In spite of having a similar synaptic potentiation to controls (Figure 6B), Kv4.2 knockout neurons showed an impaired PSA potentiation throughout the recording period (Figure 6C), and strikingly, in the latest phase of the recording where the stimulation was adjusted, the PSA potentiation was almost completely abolished (Figure 6C, $t(19) = 3.266$ $p = 0.0041$, t test Kv4.2 wild type vs. Kv4.2 knockout), indicating an essential function of the channel in controlling the EPSPspike coupling. Alike Kv4.2 knockouts, the pharmacological blockade of A-type channels in wild-type animals occluded the plasticity of intrinsic excitability (Figures S8A–S8C; PSA values after readjusting the stimulation intensity to match the fEPSP slope values recorded at baseline: 260.679 ± 49.520% and 73.142 ± 9.251% for control and 4-AP, respectively; $t(14) = 5.628$ $p < 0.0001$, t test control vs. 4-AP). In Kv4.3 knockout cells, plastic properties were on the other hand similar to controls (Figure S9) with 60% of PSA potentiation not explained by the synaptic potentiation (Figure S9).

Similar investigations of the lateral perforant path revealed that the theta burst stimulation elicited much less changes in general. The synaptic potentiation one hour after the protocol in slices from wild-type mice was only 110–115% and the PSA rather remained unchanged (Figure S10), suggesting that the theta burst stimulation of the lateral perforant path slightly depressed the excitability of the GCs. For both Kv4.2 and Kv4.3 knockout mice, a mildly larger PSA potentiation was recorded compared to wild-type controls (Figure S10), suggesting that the theta burst stimulation of the lateral perforant path slightly increased their excitability. We observed similar results after 4-AP bath application (Figures S8D–S8F).

Collectively, these results show that the plasticity of intrinsic excitability after theta burst stimulation of the medial perforant path was significantly occluded in Kv4.2 knockout mice, demonstrating an important role of Kv4.2 channels in mediating this form of intrinsic plasticity. On the opposite, the lack of Kv4.2 channels did not alter synaptic plasticity, suggesting that the Kv4.2 channel is not essential for the induction of synaptic potentiation.

Kv4.2 knockout mice display a specific impairment in spatial pattern separation task

Pattern separation has been essentially ascribed to the DG (Aimone et al., 2011; Kesner and Rolls, 2015; Marr, 1971; Schmidt et al., 2012) and has been well modeled in the entorhinal cortex (EC)-DG network. Given the functional segregation of the EC inputs to the DG and the effects of the absence of the Kv4.2 channel in the processing of medial perforant path inputs, Kv4.2 knockout animals and their control littermates were tested in a spatial pattern separation task. For this purpose, animals were tested in a behavioral task (van Goethem et al., 2018) that uses the innate preference of rodents to explore stimuli that have encountered a change as opposed to stimuli that did not (Ennaceur and Delacour, 1988). This task tests the ability of animals to detect changes in the spatial layout of objects in different conditions of similarity associated with a low or high demand on spatial pattern separation.

During the study phase, the animals explored two identical objects placed in an open field (see STAR Methods, Figure 7A). In the test phase, the animals were re-introduced in the arena where one of the objects remained in its original position while the other was displaced along a vertical axis by 6 cm (similar location: high spatial pattern separation demand) or 12 cm (dissimilar location: low spatial pattern separation demand) farther from its original location (Figure 7A). Wild-type mice successfully learned to discriminate changes in the spatial layout of objects in both the similar and dissimilar location conditions (Figures S11B, S11E,S11G, 7B, and 7C, $t(10) = 3.278$ $p = 0.0083$, one-sample t test vs. 0 for similar condition and $t(13) = 3.919$ $p = 0.0018$, one-sample t test vs. 0 for dissimilar condition). Although Kv4.2 knockouts animals exhibited comparable capacities than control animals to distinguish large changes in the spatial configuration in the dissimilar location condition (Kv4.2 +/+: $t(13) = 3.919$ $p = 0.0018$ and Kv4.2 −/−: $t(12) = 4.266$ $p = 0.0011$, one-sample t test vs. 0; $t(25) = 0.361$ $p = 0.7211$, t test Kv4.2 +/+ vs. Kv4.2 −/−), these animals were significantly impaired in their capability to detect the small changes of the spatial layout of objects in the similar location condition (Figures S11C, S11F, S11H, 7B, and 7C Kv4.2 −/−: $t(12) = 1.748$ $p = 0.1060$, one-sample t test vs. 0). Thus, the discrimination ratio of Kv4.2 knockouts was significantly lower roughly one-third of the one from wild types in the task with the highest spatial pattern separation demand (Figures 7B and 7C $t(22) = 2.557$ $p = 0.0180$, t test Kv4.2 +/+ vs. Kv4.2 −/−). This particular impairment of the Kv4.2 knockouts in discriminating very similar spatial information points to a deficit in a DG-dependent spatial pattern separation.

Object recognition memory mostly relies on the perirhinal/LEC (Deshmukh and Knierim, 2011; Deshmukh et al., 2012; Miranda et al., 2017). To ensure that the deficit in pattern separation of mice lacking the Kv4.2 channel was specific to spatial information, mice were also tested in a non-spatial version of the task, in which they had to detect changes within objects that shared different degrees of similarity. During the study phase, two identical objects were presented, while in the test phase, one of the objects was replaced by a new object that either shared a low (dissimilar pair) or high (similar pair) level of similarity compared to the other one. Thus, the pattern separation demand in the similar pair is higher than that in the dissimilar pair. The similar condition was inspired from previous studies in humans (Reagh and Yassa, 2014) and animals (Smith et al., 2014) that used a comparable experimental paradigm. Kv4.2 knockout mice could successfully detect which object was novel in the test phase, independently of the level of similarity between the objects (Figures 7D–7F, similar condition: $t(7) = 4.336$ $p = 0.0034$ and $t(10) = 6.888$ $p < 0.0001$ for Kv4.2 +/+ and Kv4.2 −/− respectively, one-sample t test vs. 0; and for the dissimilar condition: $t(7) = 4.287$ $p = 0.0036$ and $t(11) = 2.832$ $p = 0.0163$ for Kv4.2 +/+ and Kv4.2 −/− respectively, one-sample t

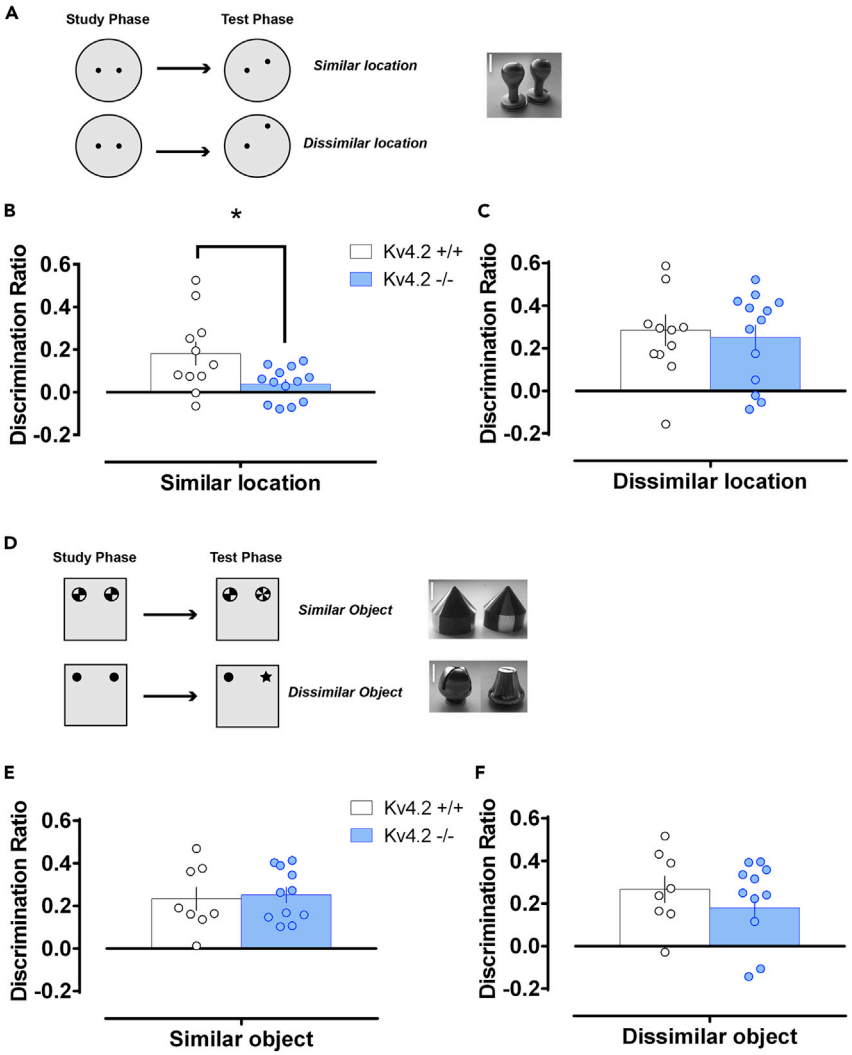

Figure 7. Kv4.2 knockout results in an impairment in spatial pattern separation task

(A) Scheme of the settings of the experiment for the spatial pattern separation task for both the similar and dissimilar conditions.

(B) Kv4.2 knockout mice (n = 13) were impaired in their ability to discriminate highly similar locations, compared to the performance of wild types (n = 11).

(C) However, they (n = 13) performed as well as controls (n = 14) when in the dissimilar location condition.

(D) Scheme of the settings of the experiment for the non-spatial object pattern separation task for both similar and dissimilar conditions. Kv4.2 knockout mice performed at similar levels than controls when discriminating both (E) similar (Kv4.2 +/+ n = 8, Kv4.2 −/− n = 11) and (F) dissimilar (Kv4.2 +/+ n = 8, Kv4.2 −/− n = 12) objects. Scale bars, 2 cm. Data are represented as mean ± SEM. *: $p < 0.05$, t test.

test vs. 0) and performance did not differ from wild type (Figures S12 and 7D–7F, $t(17) = 0.2873$ $p = 0.7773$ and $t(18) = 0.9395$ $p = 0.3599$ in similar and dissimilar conditions, respectively, t test Kv4.2 +/+ vs. Kv4.2 −/−). This observation demonstrates the specificity of the Kv4.2 channel in enabling spatial pattern separation while object-recognition memory is fully preserved in the absence of the channel.

Altogether, the results obtained from behavioral experiments suggest that the Kv4.2 channel is selectively essential for the discrimination of similar spatial information requiring a high demand on spatial pattern separation but is not involved in object recognition memory.

DISCUSSION

In this study, we found that Kv4.2 channels in the dendrites of mature GCs significantly dampen the impact of medial perforant path synapses, limit the backpropagation of action potentials into medial dendritic segments, and are key elements in the intrinsic plasticity elicited after medial perforant path stimulation. Collectively, the data show that the Kv4.2 channel is an input-specific modulator of MEC inputs. Strikingly, animals lacking the Kv4.2 channels were specifically impaired in a spatial pattern separation task. Altogether, these data point to the role of intrinsic excitability in supporting the mnemonic function of mature GCs and to the Kv4.2 channel as a potentially newly identified cellular candidate promoting the spatial pattern separation function in the DG.

Regulation of intrinsic excitability is required for memory in mature GCs

Neurons receive thousands of synapses on their dendrites. As a consequence of the integration of these inputs, synaptic transients travel along the dendrites and ultimately propagate until the soma/proximal axon where action potentials are fired or not. Dendrites are however described as anything but mere passive cables in most neurons (Stuart and Spruston, 2015). Early observations suggested that mature GC dendrites exhibited relatively negligible active properties with a weak contribution of voltage-dependent sodium or potassium conductances to GC dendritic integration (Krueppel et al., 2011). This view has been challenged by recent finding proposing the A-type current as an important regulator of the electrical features of mature GC dendrites (Kim et al., 2018; Lopez-Rojas et al., 2016). Hence, our data demonstrating the role of the Kv4.2 channels in regulating the excitability of mature GC proximal dendrites together with the anatomical segregation of the entorhinal cortex inputs onto mature neuron's dendrites underscore the potential relevance of intrinsic plasticity as an input-specific modulator of the incoming information.

The ability of dendrites to backpropagate action potentials is essential for the induction of some types of synaptic plasticity (Debanne et al., 1994; Gasparini et al., 2007; Gustafsson et al., 1987; Magee and Johnston, 1997). In addition, synaptic activity is known to activate certain kinases that functionally downregulate the Kv4.2 channel (Frick et al., 2004; Hammond et al., 2008; Kim et al., 2007). Hence, activity-dependent phosphorylation of the channel might underlie the synapse-to-soma electrical coupling reinforcement necessary for a better integration of MEC inputs. This process could potentially facilitate the induction of subsequent synaptic plasticity at the MEC-DG synapse by positively affecting the bAP. Strikingly, the absence of the Kv4.2 channel did not alter synaptic long-term potentiation but only intrinsic plasticity indicating that Kv4.2 channel is the molecular target by which the plasticity induction protocol regulates the synapse-to-soma electrical coupling. As there is no evidence for a gradient of distribution of Kv4.2 or Kv4.3 channels along the mature GC's dendrites (Alfaro-Ruíz et al., 2019; Monaghan et al., 2008; Serodio and Rudy, 1998), the segregated action of Kv4.2 channels is most likely supported by its local modulation through post-translational modifications and/or association with auxiliary subunits (Duménieu et al., 2017; Frick and Johnston, 2005; Trimmer, 2015). Indeed, PKA-mediated phosphorylation of the channel induces activity-dependent downregulation of the channel (Frick et al., 2004; Hammond et al., 2008), a mechanism that could mediate the negative regulation of the Kv4.2 channel in a context of synaptic activity.

Furthermore, the data obtained from the cFos-reporter mice suggest that an *in vivo* experience locally alter dendritic excitability of mature GCs, as already reported for CA1 (Makara et al., 2009). In mature GC's dendrites, EE seems to specifically affect the processing features of the dendritic region receiving MEC inputs, potentially through regulation of the Kv4.2 channel activity. Although this observation suggests that regulation of the Kv4.2 channel activity might be necessary for the encoding of an *in vivo* experience—and notably spatial information—further experiments are needed to nail down the link between EE-mediated regulation of medial dendrites excitability and the Kv4.2 channels.

Surprisingly, no major regulatory function of the Kv4.3 channel on intrinsic excitability could be observed in our study. Previous work on cortical pyramidal cells has reported that the duration of the action potential (or action potential width) was partly controlled by Kv4.3 channels (Carrasquillo et al., 2012), as also reported here. Because the modulatory action of this channel could be associated to certain types of activity that are beyond the scope of this study, precise conclusions regarding the Kv4.3 channel cannot be drawn. Nevertheless, the lack of effect on the excitability of mature GCs missing the expression of the Kv4.3 channel emphasizes the role of the Kv4.2 channel as a specific modulator of the MEC inputs.

Kv4.2 channel as a new cellular player for spatial pattern separation in the DG

Impairments in pattern separation have been observed in several pathological conditions and can lead to overgeneralization and maladaptive behavior (Das et al., 2014; Reagh and Yassa, 2014; Stark et al., 2010). The pattern separation function of the DG has been mainly tackled at the behavioral and network activity levels (Danielson et al., 2016; Knierim James et al., 2014; McHugh et al., 2007; Schmidt et al., 2012) and is nowadays well modeled in the EC-DG circuit (Knierim and Neunuebel, 2016). However, only few studies have so far identified cellular players essential for pattern separation in the DG (Bekinschtein et al., 2013; Kannangara et al., 2015), a step of outmost interest to get deeper insights on the neurobiological underpinnings of pattern separation. Importantly, the basal somatic electrical properties as well as the intrinsic plasticity of distal dendrites of mature GCs were largely preserved on both the Kv4.2 and Kv4.3 knockouts animals. These observations rule out a role of A-type potassium channel in controlling lateral perforant path input integration and plead in favor of an input-specific role of the Kv4.2 channel. In addition, we show that the absence of the Kv4.2 channel is selectively associated with a deficit in behavioral task involving discrimination of highly similar spatial information, suggesting a key role for the Kv4.2 channel supporting spatial pattern separation in the DG. Hypothetically, it could be that only mature GCs receiving relevant MEC inputs able to trigger the postsynaptic downregulation of the Kv4.2 channels would process this information, thereby shaping the DG network supporting a specific spatial memory. The seemingly unaltered general somatic excitability of Kv4.2 knockout GCs and the specific impairment of the spatial discrimination are at contrast with recent findings about the role of Kv4.1 channels on DG pattern separation (Kim et al., 2020). By selectively modulating the excitability of GC medial dendrites—and not the overall excitability—Kv4.2 channels also selectively impact on the spatial discrimination capability of the animals. Kv4.1 channels, on the other hand, due to their modulation of general GC somatic excitability supposedly have a less selective impact on pattern separation—in principle affecting both spatial and non-spatial pattern separation—and on general DG function.

MEC provides essential information to the DG to solve spatial pattern separation task

Besides the role of the Kv4.2 channel in modulating the signal transmission at the MEC-mature GC connection, behavioral data presented here encourage the notion that correct integration of medial perforant path inputs is essential for discrimination of highly similar spatial information, as recently suggested (Tennant et al., 2018). Several spatially tuned cells in the MEC support its central function in spatial memory (Fyhn et al., 2004; Hafting et al., 2005; Hargreaves et al., 2005; Sasaki et al., 2015). However, a population of LEC neurons, called "object-trace cells", encodes the location where an object has been previously encountered (Tsao et al., 2013), indicating that spatial aspects related to objects are not necessarily processed by the MEC. Nevertheless, the encoding of object information that rather depends on the LEC/perirhinal cortex (Deshmukh and Knierim, 2011; Deshmukh et al., 2012; Miranda et al., 2017) and presumably on the intrinsic and plastic properties of mature GC distal dendrites was fully preserved in the Kv4.2 knockout animals. Although a plausible function of the LEC object-trace cells in discriminating objects location cannot be completely ruled out, the fact that object recognition memory in Kv4.2 knockout animals remained intact argues in favor of MEC inputs as a crucial source of information to solve the spatial pattern separation task. Therefore, our results support the notion that the MEC and LEC carry different kinds of information into the hippocampus, with the largest spatial component being conveyed by the MEC (Beer et al., 2013; Eichenbaum and Lipton, 2008; Eichenbaum et al., 2007; Knierim James et al., 2014; Sauvage et al., 2013; Tennant et al., 2018) that transmit essential information for DG-dependent spatial memory.

Collectively, the data presented in this study suggest an essential function of the DG in performing spatial pattern separation and point to the Kv4.2 channel as an input-specific regulator of the MEC-driven spatial information in the DG.

Limitations of the study

Because of the absence of cell-type specificity in the mouse model employed in this work, the behavioral findings must be analyzed with caution. Nevertheless, several studies support the notion that Kv4.2 channels in mature DG GCs mediate spatial pattern separation. First, even though recent investigations show direct involvement of DG mossy cells in the pattern separation process (Danielson et al., 2017; GoodSmith et al., 2017; Scharfman, 2018; Senzai and Buzsáki, 2017), no significant level of expression of the Kv4.2 channel in the hilus of the DG was found (Alfaro-Ruíz et al., 2019; Monaghan et al., 2008), rending unlikely their direct involvement in our behavioral observations. Second, while immature GCs have long been thought to be key players in pattern separation, a couple of studies cast doubts on their ability to mediate spatial

pattern separation due to their poor functional connectivity, especially with the MEC (Dieni et al., 2016; Woods et al., 2018). Third, although the dataset presented in this study cannot fully exclude potential compensatory changes in channels expression/function in this knockout animal model, synaptic proteins and potassium channels like Kv4.3, Kv3.4, and Kv1.4, among other channels, are not significantly altered in Kv4.2 knockout mice (Chen et al., 2006). Additionally, the seemingly normal global excitability and morphology of GCs of Kv4.2 knockouts, together with the layer-specific effects on dendritic excitability and concomitant specific impairment of spatial pattern separation, advocate for a likely effect of Kv4.2. However, it should be emphasized that even though our results suggest a causal relationship between the excitability in GC medial dendrites and the spatial pattern separation capability of the animals, further experiments are necessary to corroborate this assumption.

STAR★METHODS

Detailed methods are provided in the online version of this paper and include the following:

- KEY RESOURCES TABLE
- RESOURCE AVAILABILITY
  - Lead contact
  - Materials availability
  - Data and code availability
- EXPERIMENTAL MODEL AND SUBJECT DETAILS
- METHOD DETAILS
  - Single cell recordings
  - Field recordings
  - Golgi-Cox staining
  - Behavioral tasks
- QUANTIFICATION AND STATISTICAL ANALYSIS

SUPPLEMENTAL INFORMATION

Supplemental information can be found online at https://doi.org/10.1016/j.isci.2021.102876.

ACKNOWLEDGMENTS

This study is supported by grants from the Deutsche Forschungsgemeinschaft (DFG Kr1879/5-1/6-1, DFG CRC 1436 TPA4, and SFB779 TPB8), DIP grant to M.R.K., and WGL (Pakt f. Forschung 2015) to J.L.R. We are grateful to Eike Budinger for providing help and advice with the morphological analysis. We gratefully acknowledge the excellent technical assistance of Diana Koch, Monika Marunde, and Janet Stallmann.

AUTHOR CONTRIBUTIONS

M.O., E.A., M.M.S., M.R.K., and J.L.-R. designed the experiments. M.O., E.A., T.M.. and J.L.-R. performed the experiments. M.O., E.A., T.M.W., T.M.. and J.L.-R. analyzed the data. M.O., E.A., M.M.S., M.R.K.. and J.L.-R. wrote the manuscript with assistance from all authors.

DECLARATION OF INTERESTS

The authors declare no competing interests.

Received: February 12, 2021
Revised: April 22, 2021
Accepted: July 14, 2021
Published: August 20, 2021

REFERENCES

Aimone, J.B., Deng, W., and Gage, F.H. (2011). Resolving new memories: a critical look at the dentate gyrus, adult neurogenesis, and pattern separation. Neuron *70*, 589–596.

Alfaro-Ruíz, R., Aguado, C., Martín-Belmonte, A., Moreno-Martínez, A.E., and Luján, R. (2019). Expression, cellular and subcellular localisation of Kv4.2 and Kv4.3 channels in the rodent Hippocampus. Int. J. Mol. Sci. *20*, 246.

Alme, C.B., Buzzetti, R.A., Marrone, D.F., Leutgeb, J.K., Chawla, M.K., Schaner, M.J., Bohanick, J.D., Khoboko, T., Leutgeb, S., Moser, E.I., et al. (2010). Hippocampal granule cells opt for early retirement. Hippocampus *20*, 1109–1123.

Amaral, D.G., Scharfman, H.E., and Lavenex, P. (2007). The dentate gyrus: fundamental

neuroanatomical organization (dentate gyrus for dummies). Prog. Brain Res. *163*, 3–790.

Barth, A.L., Gerkin, R.C., and Dean, K.L. (2004). Alteration of neuronal firing properties after in vivo experience in a FosGFP transgenic mouse. J. Neurosci. *24*, 6466–6475.

Beer, Z., Chwiesko, C., Kitsukawa, T., and Sauvage, M.M. (2013). Spatial and stimulus-type tuning in the LEC, MEC, POR, PrC, CA1, and CA3 during spontaneous item recognition memory. Hippocampus *23*, 1425–1438.

Bekinschtein, P., Kent, B.A., Oomen, C.A., Clemenson, G.D., Gage, F.H., Saksida, L.M., and Bussey, T.J. (2013). BDNF in the dentate gyrus is required for consolidation of "pattern-separated" memories. Cell Rep. *5*, 759–768.

Campanac, E., and Debanne, D. (2008). Spike timing-dependent plasticity: a learning rule for dendritic integration in rat CA1 pyramidal neurons. J. Physiol. *586*, 779–793.

Carrasquillo, Y., Burkhalter, A., and Nerbonne, J.M. (2012). A-type K+ channels encoded by Kv4.2, Kv4.3 and Kv1.4 differentially regulate intrinsic excitability of cortical pyramidal neurons. J. Physiol. *590*, 3877–3890.

Chavlis, S., Petrantonakis, P.C., and Poirazi, P. (2017). Dendrites of dentate gyrus granule cells contribute to pattern separation by controlling sparsity. Hippocampus *27*, 89–110.

Chen, X., Yuan, L.L., Zhao, C., Birnbaum, S.G., Frick, A., Jung, W.E., Schwarz, T.L., Sweatt, J.D., and Johnston, D. (2006). Deletion of Kv4.2 gene eliminates dendritic A-type K+ current and enhances induction of long-term potentiation in hippocampal CA1 pyramidal neurons. J. Neurosci. *26*, 12143–12151.

Danielson, N.B., Kaifosh, P., Zaremba, J.D., Lovett-Barron, M., Tsai, J., Denny, C.A., Balough, E.M., Goldberg, A.R., Drew, L.J., Hen, R., et al. (2016). Distinct contribution of adult-born hippocampal granule cells to context encoding. Neuron *90*, 101–112.

Danielson, N.B., Turi, G.F., Ladow, M., Chavlis, S., Petrantonakis, P.C., Poirazi, P., and Losonczy, A. (2017). In vivo imaging of dentate gyrus mossy cells in behaving mice. Neuron *93*, 552–559.e4.

Das, T., Ivleva, E.I., Wagner, A.D., Stark, C.E.L., and Tamminga, C.A. (2014). Loss of pattern separation performance in schizophrenia suggests dentate gyrus dysfunction. Schizophr. Res. *159*, 193–197.

Debanne, D., Gähwiler, B.H., and Thompson, S.M. (1994). Asynchronous pre- and postsynaptic activity induces associative long-term depression in area CA1 of the rat hippocampus in vitro. Proc. Natl. Acad. Sci. U S A *91*, 1148–1152.

Debanne, D., Inglebert, Y., and Russier, M. (2019). Plasticity of intrinsic neuronal excitability. Curr. Opin. Neurobiol. *54*, 73–82.

Deshmukh, S.S., and Knierim, J.J. (2011). Representation of non-spatial and spatial information in the lateral entorhinal cortex. Front. Behav. Neurosci. *5*, *69*.

Deshmukh, S.S., Johnson, J.L., and Knierim, J.J. (2012). Perirhinal cortex represents nonspatial, but not spatial, information in rats foraging in the presence of objects: comparison with lateral entorhinal cortex. Hippocampus *22*, 2045–2058.

Dieni, C.V., Panichi, R., Aimone, J.B., Kuo, C.T., Wadiche, J.I., and Overstreet-Wadiche, L. (2016). Low excitatory innervation balances high intrinsic excitability of immature dentate neurons. Nat. Commun. *7*, 11313.

Duménieu, M., Oulé, M., Kreutz, M.R., and Lopez-Rojas, J. (2017). The segregated expression of voltage-gated potassium and sodium channels in neuronal membranes: functional implications and regulatory mechanisms. Front. Cell. Neurosci. *11*, 115.

Eichenbaum, H., and Lipton, P.A. (2008). Towards a functional organization of the medial temporal lobe memory system: role of the parahippocampal and medial entorhinal cortical areas. Hippocampus *18*, 1314–1324.

Eichenbaum, H., Yonelinas, A.P., and Ranganath, C. (2007). The medial temporal lobe and recognition memory. Annu. Rev. Neurosci. *30*, 123–152.

Ennaceur, A., and Delacour, J. (1988). A new one-trial test for neurobiological studies of memory in rats. 1: behavioral data. Behav. Brain Res. *31*, 47–59.

Espinoza, C., Guzman, S.J., Zhang, X., and Jonas, P. (2018). Parvalbumin + interneurons obey unique connectivity rules and establish a powerful lateral-inhibition microcircuit in dentate gyrus. Nat. Commun. *9*, 1–10.

Frick, A., and Johnston, D. (2005). Plasticity of dendritic excitability. J. Neurobiol. *64*, 100–115.

Frick, A., Magee, J., and Johnston, D. (2004). LTP is accompanied by an enhanced local excitability of pyramidal neuron dendrites. Nat. Neurosci. *7*, 126–135.

Fyhn, M., Molden, S., Witter, M.P., Moser, E.I., and Moser, M.-B. (2004). Spatial representation in the entorhinal cortex. Science *305*, 1258–1264.

Gasparini, S., Losonczy, A., Chen, X., Johnston, D., and Magee, J.C. (2007). Associative pairing enhances action potential back-propagation in radial oblique branches of CA1 pyramidal neurons. J. Physiol. *580*, 787–800.

van Goethem, N.P., van Hagen, B.T.J., and Prickaerts, J. (2018). Assessing spatial pattern separation in rodents using the object pattern separation task. Nat. Protoc. *13*, 1763–1792.

GoodSmith, D., Chen, X., Wang, C., Kim, S.H., Song, H., Burgalossi, A., Christian, K.M., and Knierim, J.J. (2017). Spatial representations of granule cells and mossy cells of the dentate gyrus. Neuron *93*, 677–690.e5.

Gustafsson, B., Wigström, H., Abraham, W.C., and Huang, Y.Y. (1987). Long-term potentiation in the hippocampus using depolarizing current pulses as the conditioning stimulus to single volley synaptic potentials. J. Neurosci. *7*, 774–780.

Hafting, T., Fyhn, M., Molden, S., Moser, M.-B., and Moser, E.I. (2005). Microstructure of a spatial map in the entorhinal cortex. Nature *436*, 801–806.

Hammond, R.S., Lin, L., Sidorov, M.S., Wikenheiser, A.M., and Hoffman, D.A. (2008). Protein kinase a mediates activity-dependent Kv4.2 channel trafficking. J. Neurosci. *28*, 7513–7519.

Hargreaves, E.L., Rao, G., Lee, I., and Knierim, J.J. (2005). Major dissociation between medial and lateral entorhinal input to dorsal hippocampus. Science *308*, 1792–1794.

Hoffman, D.A., Magee, J.C., Colbert, C.M., and Johnston, D. (1997). K+ channel regulation of signal propagation in dendrites of hippocampal pyramidal neurons. Nature *387*, 869–875.

Jung, M.W., and McNaughton, B.L. (1993). Spatial selectivity of unit activity in the hippocampal granular layer. Hippocampus *3*, 165–182.

Kannangara, T.S., Eadie, B.D., Bostrom, C.A., Morch, K., Brocardo, P.S., and Christie, B.R. (2015). GluN2A-/- mice lack bidirectional synaptic plasticity in the dentate gyrus and perform poorly on spatial pattern separation tasks. Cereb. Cortex *25*, 2102–2113.

Kesner, R.P., and Rolls, E.T. (2015). A computational theory of hippocampal function, and tests of the theory. Neurosci. Biobehav Rev. *48*, 92–147.

Kim, J., Wei, D.S., and Hoffman, D.A. (2005). Kv4 potassium channel subunits control action potential repolarization and frequency-dependent broadening in rat hippocampal CA1 pyramidal neurones. J. Physiol. *569*, 41–57.

Kim, J., Jung, S.C., Clemens, A.M., Petralia, R.S., and Hoffman, D.A. (2007). Regulation of dendritic excitability by activity-dependent trafficking of the A-type K+ channel subunit Kv4.2 in hippocampal neurons. Neuron *54*, 933–947.

Kim, K.-R., Lee, S.Y., Yoon, S.H., Kim, Y., Jeong, H.-J., Lee, S., Suh, Y.H., Kang, J.-S., Cho, H., Lee, S.-H., et al. (2020). Kv4.1, a key ion channel for low frequency firing of dentate granule cells, is crucial for pattern separation. J. Neurosci. *40*, 2200–2214.

Kim, S., Kim, Y., Lee, S.-H., and Ho, W.-K. (2018). Dendritic spikes in hippocampal granule cells are necessary for long-term potentiation at the perforant path synapse. Elife *7*, e35269.

Knierim, J.J., and Neunuebel, J.P. (2016). Tracking the flow of hippocampal computation: pattern separation, pattern completion, and attractor dynamics. Neurobiol. Learn. Mem. *129*, 38–49.

Knierim James, J., Neunuebel Joshua, P., and Deshmukh Sachin, S. (2014). Functional correlates of the lateral and medial entorhinal cortex: objects, path integration and local–global reference frames. Philos. Trans. R. Soc. B Biol. Sci. *369*, 20130369.

Koyama, R. (2016). Dentate circuitry as a model to study epileptogenesis. Biol. Pharm. Bull. *39*, 891–896.

Krueppel, R., Remy, S., and Beck, H. (2011). Dendritic integration in hippocampal dentate granule cells. Neuron *71*, 512–528.

Lai, H.C., and Jan, L.Y. (2006). The distribution and targeting of neuronal voltage-gated ion channels. Nat. Rev. Neurosci. *7*, 548–562.

Leutgeb, J.K., Leutgeb, S., Moser, M.B., and Moser, E.I. (2007). Pattern separation in the dentate gyrus and CA3 of the hippocampus. Science *315*, 961–966.

Lopez-Rojas, J., Heine, M., and Kreutz, M.R. (2016). Plasticity of intrinsic excitability in mature granule cells of the dentate gyrus. Sci. Rep. *6*, 21615.

Madar, A.D., Ewell, L.A., and Jones, M.V. (2019). Pattern separation of spiketrains in hippocampal neurons. Sci. Rep. *9*, 1–20.

Magee, J.C., and Johnston, D. (1997). A synaptically controlled, associative signal for Hebbian plasticity in hippocampal neurons. Science *275*, 209–213.

Makara, J.K., Losonczy, A., Wen, Q., and Magee, J.C. (2009). Experience-dependent compartmentalized dendritic plasticity in rat hippocampal CA1 pyramidal neurons. Nat. Neurosci. *12*, 1485–1487.

Marr, D. (1971). Simple memory: a theory for archicortex. Philos. Trans. R. Soc. Lond. B Biol. Sci. *262*, 23–81.

McHugh, T.J., Jones, M.W., Quinn, J.J., Balthasar, N., Coppari, R., Elmquist, J.K., Lowell, B.B., Fanselow, M.S., Wilson, M.A., and Tonegawa, S. (2007). Dentate gyrus NMDA receptors mediate rapid pattern separation in the hippocampal network. Science *317*, 94–99.

Miranda, M., Kent, B.A., Morici, J.F., Gallo, F., Weisstaub, N.V., Saksida, L.M., Bussey, T.J., and Bekinschtein, P. (2017). Molecular mechanisms in perirhinal cortex selectively necessary for discrimination of overlapping memories, but independent of memory persistence. ENeuro *4*, ENEURO.0293-17.2017.

Monaghan, M.M., Menegola, M., Vacher, H., Rhodes, K.J., and Trimmer, J.S. (2008). Altered expression and localization of hippocampal A-type potassium channel subunits in the pilocarpine-induced model of temporal lobe epilepsy. Neuroscience *156*, 550–562.

Mylius, J., Brosch, M., Scheich, H., and Budinger, E. (2013). Subcortical auditory structures in the Mongolian gerbil: I. Golgi architecture. J. Comp. Neurol. *521*, 1289–1321.

Pernia-Andrade, A.J., and Jonas, P. (2014). Theta-gamma-modulated synaptic currents in hippocampal granule cells in vivo define a mechanism for network oscillations. Neuron *81*, 140–152.

Reagh, Z.M., and Yassa, M.A. (2014). Object and spatial mnemonic interference differentially engage lateral and medial entorhinal cortex in humans. Proc. Natl. Acad. Sci. U S A *111*, E4264–E4273.

Remy, S., Beck, H., and Yaari, Y. (2010). Plasticity of voltage-gated ion channels in pyramidal cell dendrites. Curr. Opin. Neurobiol. *20*, 503–509.

Sasaki, T., Leutgeb, S., and Leutgeb, J.K. (2015). Spatial and memory circuits in the medial entorhinal cortex. Curr. Opin. Neurobiol. *32*, 16–23.

Sauvage, M.M., Nakamura, N.H., and Beer, Z. (2013). Mapping memory function in the medial temporal lobe with the immediate-early gene Arc. Behav. Brain Res. *254*, 22–33.

Scharfman, H.E. (2018). Advances in understanding hilar mossy cells of the dentate gyrus. Cell Tissue Res. *373*, 643–652.

Schmidt, B., Marrone, D.F., and Markus, E.J. (2012). Disambiguating the similar: the dentate gyrus and pattern separation. Behav. Brain Res. *226*, 56–65.

Schmidt-Hieber, C., Jonas, P., and Bischofberger, J. (2004). Enhanced synaptic plasticity in newly generated granule cells of the adult hippocampus. Nature *429*, 184–187.

Senzai, Y., and Buzsáki, G. (2017). Physiological properties and behavioral correlates of hippocampal granule cells and mossy cells. Neuron *93*, 691–704.e5.

Serodio, P., and Rudy, B. (1998). Differential expression of Kv4 K+ channel subunits mediating subthreshold transient K+ (A-type) currents in rat brain. J. Neurophysiol. *79*, 1081–1091.

Smith, G.K., Kesner, R.P., and Korenberg, J.R. (2014). Dentate gyrus mediates cognitive function in the Ts65Dn/DnJ mouse model of down syndrome: DG Mediates Cognition in Mouse Model of DS. Hippocampus *24*, 354–362.

Staley, K.J., Otis, T.S., and Mody, I. (1992). Membrane properties of dentate gyrus granule cells: comparison of sharp microelectrode and whole-cell recordings. J. Neurophysiol. *67*, 1346–1358.

Stark, S.M., Yassa, M.A., and Stark, C.E.L. (2010). Individual differences in spatial pattern separation performance associated with healthy aging in humans. Learn. Mem. *17*, 284–288.

Stuart, G.J., and Spruston, N. (2015). Dendritic integration: 60 years of progress. Nat. Neurosci. *18*, 1713–1721.

Tennant, S.A., Fischer, L., Garden, D.L.F., Gerlei, K.Z., Martinez-Gonzalez, C., McClure, C., Wood, E.R., and Nolan, M.F. (2018). Stellate cells in the medial entorhinal cortex are required for spatial learning. Cell Rep. *22*, 1313–1324.

Titley, H.K., Brunel, N., and Hansel, C. (2017). Toward a neurocentric view of learning. Neuron *95*, 19–32.

Trimmer, J.S. (2015). Subcellular localization of K+ channels in mammalian brain neurons: remarkable precision in the midst of extraordinary complexity. Neuron *85*, 238–256.

Truchet, B., Manrique, C., Sreng, L., Chaillan, F.A., Roman, F.S., and Mourre, C. (2012). Kv4 potassium channels modulate hippocampal EPSP-spike potentiation and spatial memory in rats. Learn. Mem. *19*, 282–293.

Tsao, A., Moser, M.-B., and Moser, E.I. (2013). Traces of experience in the lateral entorhinal cortex. Curr. Biol. *23*, 399–405.

Wang, C., Chen, X., Lee, H., Deshmukh, S.S., Yoganarasimha, D., Savelli, F., and Knierim, J.J. (2018). Egocentric coding of external items in the lateral entorhinal cortex. Science *362*, 945–949.

Watanabe, S., Hoffman, D.A., Migliore, M., and Johnston, D. (2002). Dendritic K+ channels contribute to spike-timing dependent long-term potentiation in hippocampal pyramidal neurons. Proc. Natl. Acad. Sci. U S A *99*, 8366–8371.

Witter, M.P. (2007). The perforant path: projections from the entorhinal cortex to the dentate gyrus. In Progress in Brain Research, E.S. Helen, ed. (Elsevier), pp. 43–61.

Woods, N.I., Vaaga, C.E., Chatzi, C., Adelson, J.D., Collie, M.F., Perederiy, J.V., Tovar, K.R., and Westbrook, G.L. (2018). Preferential targeting of lateral entorhinal inputs onto newly integrated granule cells. J. Neurosci. *38*, 5843–5853.

Yang, S., Tang, C.-M., and Yang, S. (2015). The shaping of two distinct dendritic spikes by A-type voltage-gated K(+) channels. Front. Cell. Neurosci. *9*, 469.

Yassa, M.A., and Stark, C.E. (2011). Pattern separation in the hippocampus. Trends Neurosci. *34*, 515–525.

STAR★METHODS

KEY RESOURCES TABLE

REAGENT or RESOURCE	SOURCE	IDENTIFIER
Chemicals, peptides, and recombinant proteins		
Alexa Fluor™ 594 Hydrazide	Invitrogen	Cat# A10438
Calcium sensor Fluo-5F	Invitrogen	Cat# F14221
-(−)Bicuculline methiodide	Tocris	Cat# 2503
Experimental models: organisms/strains		
Mouse: C57BL/6J	Charles River	RRID:IMSR_JAX:000664
Mouse: Kv4.2/Kcnd2 Knockout: Kcnd2^{tm1Jmn}	Gift from Jeanne Nerbonne (Center for Cardiovascular Research at the Washington University School of Medicine. Saint-Louis, Missouri – USA)	
Mouse: Kv4.3/Kcnd3 Knockout: Kcnd3^{em1J}	The Jackson Laboratory	Cat# 027443 (NA any longer)
Mouse: B6.Cg-Tg(Fos/EGFP)1-3Brth/J	The Jackson Laboratory	Cat#: 014135
Software and algorithms		
Patchmaster and Fitmaster	HEKA	NA
Clampex and Clampfit	Molecular Devices	NA
Minianalysis	Synaptosoft	NA
MES	Femtonics	NA

RESOURCE AVAILABILITY

Lead contact

Further information and requests for resources and reagents should be directed to and will be fulfilled by the lead contact, Jeffrey Lopez-Rojas (jl5545@columbia.edu).

Materials availability

This study did not generate unique reagents.

Data and code availability

All data and code are available from the lead contact upon request.

EXPERIMENTAL MODEL AND SUBJECT DETAILS

All experimental procedures were carried out in accordance with the EU Council Directive 2010/63/EU and were approved by the local Committee for Ethics and Animal Research (Landesverwaltungsamt Sachsen-Anhalt, Germany).

All experiments were performed on male C57BL/6J mice from Charles River that were bred in house. Kv4.2 mice were kindly provided by the lab of Jeanne Nerbonne from the Center for Cardiovascular Research at the Washington University School of Medicine (Saint-Louis, Missouri – USA). The line was sent to Janvier for rederivation through embryo transfer and further kept in a C57BL/6J background in house. Kv4.3 mice were purchased from the Jackson Laboratory with a C57BL/6NJ background and further bred in house with C57BL/6J background. The FosGFP reporter line was obtained from the Jackson laboratory and were primarily described in Barth et al. (2004). This line was kept in a C57Bl/6J background. Male mice of 11–14 weeks of age were used in all cases.

METHOD DETAILS

Single cell recordings

Hippocampal slices. Transverse 350 μm slices from the hippocampus of young adult male mice (11–13 weeks old) were cut with a vibratome (Leica VT1000S) in ice-cold ACSF solution. The ACSF

contained the following (in mM): 124 NaCl, 4.9 KCl, 2 $MgSO_4$, 2 $CaCl_2$, 1.2 KH_2PO_4, 25.6 $NaHCO_3$ and 20 glucose, equilibrated with 95% O_2/5% CO_2. Slices were incubated at 34°C for 25 min and subsequently held at room temperature. The same extracellular solution was used for preparation, incubation and holding of the slices.

Current-clamp recordings. Patch pipettes were pulled from a vertical micropipette puller (model PC-100, Narishige) and filled with an intracellular solution containing the following (in mM): 130 potassium gluconate, 20 HEPES, 2 $MgCl_2$, 2 Mg-ATP, 0.3 Na-GTP. The pH was adjusted to 7.3 and the osmolarity to 290 mOsm. Pipettes of a 6–9 MΩ tip resistance were used. The temperature in the recording chamber was adjusted to 25°C. Whole-cell patch-clamp configuration was established, and cells were held at −70 mV (for experiments measuring bAP-evoked calcium fluxes) or −63 mV (for all other experiments) by injecting a small holding current. Mature GCs were selected based on their shape, size and distribution in the two outer thirds of the GC layer. Their identity was further confirmed by their input resistance, according to the literature, below 300 MΩ (Schmidt-Hieber et al., 2004).

A 6–9 MΩ patch pipette was filled with extracellular solution and placed in the molecular layer approximately 100 μm from the cell body, targeting the MPP, or close to the hippocampal fissure to target the LPP. An ISO-Flex stimulator (A.M.P.I.) was used to deliver short square pulses of 0.2 ms duration. The extracellular solution contained 20 μM bicuculline.

For the calculation of the EPSP-threshold (E50) an E-S curve (EPSP slope vs. Spike probability) was generated by varying the strength of the synaptic stimulation in order to get a representation of the whole range: from an EPSP evoking a spike with 100% probability to sub-threshold EPSPs evoking no action potential. Around 30–50 stimuli were applied at 0.1 Hz. EPSP-slopes were measured during the first 2 ms and sorted in 0.5 Vs–1 bins. The firing probability was calculated for each bin and the E50 value was estimated by fitting the curve to a sigmoid function. The sub-threshold EPSPs in the E-S curves were used in the calculation of the EPSP-amplitude/slope ratios, that is reported for each cell as the slope of the linear fit of the EPSP-amplitude vs. EPSP-slope relation (Campanac and Debanne, 2008; Lopez-Rojas et al., 2016). For a few cells the stimulation intensity was not enough to reliable elicit action potentials and only the EPSP-amplitude/slope was quantified from the subthreshold events.

Recordings were performed with an EPC10 patch-clamp amplifier. Data were acquired and stored using Patchmaster and analyzed with Fitmaster. The voltage values were not corrected for the liquid junction potential of 13.6 mV (V_membrane = V_pipette -V_liquid junction).

Two-photon imaging. A commercial 2-photon laser-scanning Femto2D microscope from Femtonics (Budapest, Hungary) was used. Laser pulses at 810 nm were provided by a Ti:Sapphire femtosecond laser (Cameleon Ultra I, Coherent). For measuring Ca^{2+} signals, green (Fluo-5F) and red (Alexa Fluor 594) fluorescence values were collected during 500 Hz line scans. Fluorescence changes were quantified as the increase in green fluorescence normalized to the average red fluorescence (ΔG/R). The Ca^{2+} transient peaks were estimated from exponential fits of the fluorescence traces. Fluorescence was collected through the objective (60× 1.0 NA, Olympus) and the oil immersion condenser (1.4 NA, Olympus) with 2 pairs of photomultipliers (2 for collecting red band fluorescence and the other 2 for green band fluorescence). An additional photomultiplier was used to collect the transmitted infrared light. The composition of the intracellular solution for these experiments was as follows (in mM): 130 potassium gluconate, 20 HEPES, 2 $MgCl_2$, 2 Mg-ATP, 0.3 Na-GTP, 0.25 Fluo-5F and 0.01 Alexa 594. The pH was adjusted to 7.3 and the osmolarity to 290 mOsm. The extracellular solution was the same as in the other experiments and also contained 20 μM bicuculline. Fluorescence data recording started 15 min after obtaining the whole-cell configuration.

Electrophysiological recordings were performed with a Multiclamp 700B amplifier and an acquisition interface Digidata 1440A. Data were acquired and stored using Clampex and analyzed with Clampfit and Mini-analysis. Fluorescence data was acquired using the MES software (Femtonics).

Field recordings

Hippocampal slices. Field recordings were done in transversal hippocampal slices. The hippocampus was isolated in ice-cold ACSF solution. Hippocampal slices (400 μm thickness) were cut with a chopper

and placed in an interface chamber at 32°C. The ACSF solution was the same as that in the single-cell experiments. Slices were incubated for at least 3 hr before the start of the recordings, which were performed in the same incubation interface chamber at 32°C.

Electrophysiology. The population spike and the field-excitatory postsynaptic potential were measured with 2 monopolar lacquer-coated, stainless steel electrodes positioned at the GC layer and middle or outer part of the molecular layer. One stimulation electrode placed in the middle or outer part of the molecular layer was used to stimulate the medial or lateral perforant path, respectively. Biphasic constant current pulses (0.1 ms per half-wave duration) to the perforant path at 0.033 Hz evoking 25% of maximal population spike amplitude were used for test recordings.

LTP-induction protocol. The LTP-induction protocol was theta-burst stimulation (TBS) and consisted of 4 episodes repeated at 0.1 Hz; each episode included brief presynaptic bursts, that is, 10 pulses (0.2 ms per half-wave duration, with the same stimulation intensity as in baseline recordings) at 100 Hz, repeated 10 times at 5 Hz.

Golgi-Cox staining

Golgi-impregnation of the mouse brains largely correspond to those described by Mylius and coworkers (Mylius et al., 2013). Twelve weeks old mice were deeply anesthetized with an overdose of pentobarbital, exsanguinated and brains were removed and impregnated in the dark for 14 days at room temperature in 50 mL of a Golgi-Cox solution. After impregnation, brains were dehydrated in a graded series of ethanol, treated in a mixture of 100% ethanol and anhydrous diethylether for 4 hr and embedded in a graded series of celloidin. Within the next days, brain-containing celloidin blocks were formed and dried in a desiccator under exposure to phosphorus pentoxide and polymerized and hardened under exposure to chloroform. Afterward, brains were cut on a sliding microtome (Microm) into serial horizontal sections of 150 μm thickness. Sections were collected in 70% ethanol and rinsed in distilled water. Then, they were treated in a 50% alkaline ammonia solution followed by 0.5% phenylen-diamine. The staining was developed in 1% dectol and fixed in 5% tetenal. Finally, sections were rapidly dehydrated in a graded series of ethanol and xylol and mounted with Merckoglas. Sections were examined using a standard bright field microscope (Leica DMRX, Germany). Regions of interest from both hemispheres were identified. The morphology of 12 dentate GCs was reconstructed three-dimensionally with the help of a camera lucida system connected to the microscope (NeuroLucida v.11.07, NeuroExplorer v.11.03; MicroBrightField, Europe).

Behavioral tasks

Housing and habituation. For the behavioral experiments, mice were kept under an inverted light cycle for at least one week before starting any experimental manipulation. The animals had *ad libitum* access to water and food and were kept in groups to avoid isolation-related stress. Mice were handled for 5 consecutive days in the experimental room. After 2 days of rest, animals were placed once per day for 20 min in the open field (circular open field used for the spatial pattern separation task: PVC wall 50 cm high and 40 cm in diameter; squared open field used for the object pattern separation task: PVC gray wall 40 cm high and 30 cm long sides) during the first 2 days and twice per day for 5 min with objects on the following 2 days for habituation.

Spatial pattern separation task. The general procedure was based on a previously described protocol (van Goethem et al., 2018). Two identical round-shaped metallic objects (height: 5cm, diameter 2cm) were used. During the study phase, the animals had the possibility to explore the arena and the objects for 15 min. The objects were placed aligned in the center of the arena at 12 cm from the wall. Mice were then returned to their home cages and after a 30 min retention interval, each mouse was placed again in the open field for 6 min (test phase). During the test phase one of the objects was placed at the same location than the one used during the study phase, while the second object was placed either at 6 cm (high discrimination load) or 12 cm (low discrimination load) farther from its original location along a vertical axis. Each animal was tested for both conditions on different days (with 3 days in between). In order to avoid any biased results due to side preferences, the new position in the arena during the test phase was randomized across trials.

Non-spatial object pattern separation task. Seven days after the spatial discrimination task, the mice were habituated to the new open field following the habituation procedure described above. During the

study phase the animals were allowed to explore for 15 min the arena and two identical objects were placed on adjacent corners of the arena. Mice were then returned to their home cages and after a 30 min retention interval, each mouse was placed again in the open field for 6 min (test phase). In this test phase, one object from the study phase was presented (reference object) while the second object was new and shared a certain degree of similarity with the reference object (similar condition: high discrimination demand; dissimilar condition: low discrimination demand).

Analysis. Performance was scored manually by 2 independent experimenters blind to experimental conditions and averaged. A mouse was considered to explore an object if it was facing the object at a distance of no more than 2 cm or when it was directly interacting with the object (licking, sniffing). Climbing, sitting on or biting the objects were not considered as exploratory behavior. The discrimination ratio during the test phase was calculated using this formula: [(Exploration Time for the New Location or New Object) – (Exploration Time for the Reference Location or Reference Object)]/Total Exploration Time, where the Total Exploration Time was the sum of the exploration of each object during the test phase. Animals that did not explore each object for at least 10 s during the study phase or that only briefly visited the objects (going back and forth) without interacting with them (sniffing, licking, going around) were discarded.

QUANTIFICATION AND STATISTICAL ANALYSIS

All data are presented as mean ± standard error of the mean (SEM). Power calculations were not performed *a priori*, but sample sizes are similar or greater than those generally used in the field. Statistical tests were performed using Prism 6 (GraphPad Software Inc, La Jolla, Ca, USA) and are described where appropriate in the text. In general, normality of data was tested using the Shapiro–Wilk Test. Normally distributed data were analyzed using a t test for comparison of two groups or two-way ANOVA, followed by multiple-comparisons post hoc test, for comparison of more than two groups.